Os(II) Based Green to Red Phosphors: A Great Prospect for Solution-Processed, Highly Efficient Organic Light-Emitting Diodes

Bo-Sian Du, Jia-Ling Liao, Ming-Hong Huang, Cheng-Huei Lin, Hao-Wu Lin, Yun Chi,*, Hsiao-An Pan, Gang-Lun Fan, Ken-Tsung Wong, Gene-Hsiang Lee, and Pi-Tai Chou**

Preparation and characterization of a new class of emissive Os(II) complexes (1–5) have been achieved using 3-(thiazol-2-yl), 3-(benzothiazol-2-yl), 3-(imidazol-2-yl) and 3-(benzimidazol-2-yl) azole chelates, together with the incorporation of one diphosphine ancillary for satisfying the octahedral coordination arrangement. The resulting Os(II) complexes, except for 5, all show bright emission spanning visible region from green to saturated red, and their structural versus spectroscopic properties have been comprehended by absorption/emission together with computational approaches. Subsequently, a series of solution-processed OLEDs using 1–4 as the dopant were successfully fabricated, demonstrating excellent device performances with external quantum efficiency (EQE) of 15%, current efficiency exceeding 48 cd/A, and power conversion efficiency up to 50 lm/W. Complex 4 is the only Os(II) based phosphor so far suitable for the fabrication of highly efficient green-emitting OLEDs.

1. Introduction

Organometallic complexes possessing a third-row transition-metal element are crucial for the fabrication of highly efficient organic light emitting diodes (OLEDs).[1] The strong spin-orbit coupling induced by the heavy central metal element such as Pt(II), Os(II) and Ir(III) promotes an efficient intersystem crossing from the singlet to the triplet excited states, which then facilitates strong luminescence by the harnessing of both singlet and triplet excitons generated in the emissive layer of OLED devices. As a result, a strong emphasis has been put on the photophysical properties of these metal-based phosphors.

For the commonly studied Ir(III) phosphors, their architecture comprises of at least one cyclometalate and, thus, upon variation of the substituents or even the skeletal designs, their luminescent properties, particularly the emission wavelengths, were successfully fine-tuned according to both theoretical predictions and experimental confirmation.[2] The best understandable example is tri-substituted $Ir(ppy)_3$ which showed emission at λ_{max} 514 nm, originating from the triplet excited states possessing both ligand-centered $\pi\pi^*$ and metal-to-ligand charge transfer characters.[3] Replacement of 2-phenylisoquinoline (piqH) for 2-phenylpyridine (ppyH) in $[Ir(ppy)_3]$ gave formation of the red-emitting $[Ir(piq)_3]$, for which the greater π-conjugation of piq chelate afforded a substantial increase of emission wavelengths.[4] Conversely, conceptual substitution of 2,4-difluorophenylpyridine (dfppyH) for phenylpyridine gave the formation of FIrpic, FIr6, FIrtaz and related Ir(III) complexes;[5] all of them showed large blue-shifted emission due to the simultaneous enlargement of ligand-centered $\pi\pi^*$ energy gap and stabilization of the occupied metal-based d_π orbitals.

In yet another approach, tuning of emission wavelengths in the series of charge-neutral Os(II) phosphors was documented with limited success.[6] For representative example, the corresponding 2-isoquinolinyl pyazolate complex **A**, shown in **Scheme 1** below, exhibited a notable red-shifted emission at λ_{max} = 690 nm in CH_2Cl_2 solution versus that of λ_{max} = 584 for the 2-pyridyl pyazolate Os(II) complex **B**, supporting the general hypothesis on the reduction of emission energy gap by increasing the π-conjugation.[7] Alternatively, there is still a lack of report on how to induce the blue-shift of Os(II) emitters by destabilizing the π^* orbitals of azolate chelates, except for increasing the electron-accepting character of phosphine ancillaries; the later would exert the blue-shifting via the opposite effect of stabilizing the metal-based d_π orbitals.[8]

With an aim of finding new class of azole chelates that showed enlarged $\pi\pi^*$ gap, we proceeded to synthesize the respectively 3-(thiazol-2-yl), 3-(benzothiazol-2-yl), 3-(imidazol-2-yl) and 3-(benzimidazol-2-yl) azoles, namely:

B.-S. Du, J.-L. Liao, C.-H. Lin, Prof. Y. Chi
Department of Chemistry
National Tsing Hua University
Hsinchu 30013, Taiwan
E-mail: ychi@mx.nthu.edu.tw
M.-H. Huang, Prof. H.-W. Lin
Department of Materials Science and Engineering
National Tsing Hua University
Hsinchu 30013, Taiwan
E-mail: hwlin@mx.nthu.edu.tw
H.-A. Pan, G.-L. Fan, Prof. K.-T. Wong, G.-H. Lee, Prof. P.-T. Chou
Department of Chemistry
National Taiwan University
Taipei 10617, Taiwan
E-mail: chop@ntu.edu.tw

DOI: 10.1002/adfm.201200718

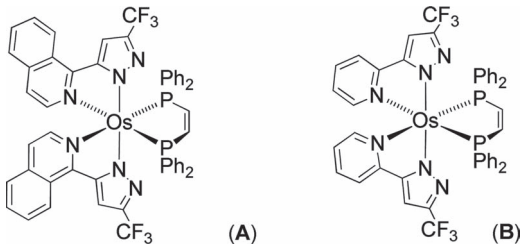

Scheme 1. Structural drawing for Os(II) complexes **A** and **B**.

5-(benzothiazol-2-yl)-3-trifluoromethylpyrazole (btfpH), 5-(thiazol-2-yl)-3-trifluoro- -methylpyrazole (tfpH), 5-(1-isopropylbenzimidazol-2-yl)-3-trifluoromethylpyrazole (ibifpH) and 5-(1-isopropylimidazol-2-yl)-3-trifluoromethylpyrazole (iifpH) (see **Scheme 2**). Their electronic character is distinctive from that of typical 2-pyridyl and 2-isoquinolinyl substituent, i.e. pypzH and iqpzH, for which the main difference resides on the greater polarizability of sulfur atom in thiazolyl fragment and the electron rich character of the trivalent nitrogen atom in the imidazolyl fragment. Thus, one should be capable of obtaining Os(II) phosphors with either red-shifted emission for thiazolyl derivatives or green emission for imidazolyl complexes. To shoot these new Os(II) phosphors for the practical applications, we also made attempts to fabricate the highly efficient OLED devices using solution based processes.

2. Results and Discussion

2.1. Synthesis and Characterization

The benzothiazol-2-yl, 1-isopropylbenzimidazol-2-yl and relevant diketones were first prepared by Claisen condensation of ethyl trifluoroacetate with 2-acetylbenzothiazole and 2-acetyl-1-isopropylbenzimidazole, respectively.[9] After then, treatment of these diketone compounds with hydrazine hydrate in refluxing ethanol and in presence of acetic acid gave the desired 5-aryl-3-trifluoromethylpyrazole chelates; namely: 5-(benzothiazol-2-yl)-3-trifluoromethylpyrazole(btfpH), 5-(thiazol-2-yl)-3-trifluoro- -methylpyrazole(tfpH) 5-(1-isopropylbenzimidazol-2-yl)-3-trifluoromethylpyrazole (ibifpH) and 5-(1-isopropylimidazol-2-yl)-3-trifluoromethylpyrazole (iifpH),

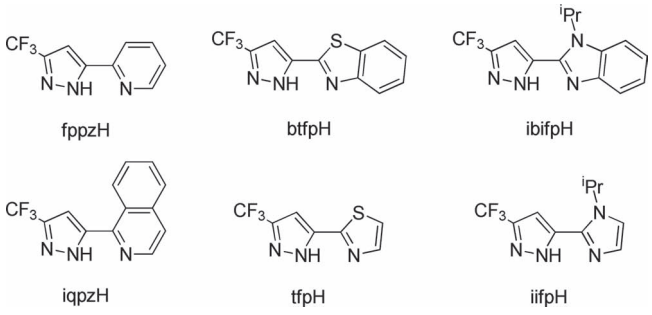

Scheme 2. Various ligand structures elaborated in this study.

respectively; for which their structural drawings are depicted in Scheme 2.

Subsequently, the synthesis of the *cis*-oriented Os(II) thiazolyl complexes $[Os(btfp)_2(dppb)]$ (**1**), $[Os(btfp)_2(pp2b)]$ (**2**) and $[Os(tfp)_2(dppb)]$ (**3**) follows the routine protocol, in which the 2-thiazolyl pyrazole ligand (i.e. btfpH or ftpH) was first treated with pulverized $Os_3(CO)_{12}$ in refluxing diethylene glycol monomethyl ether (DGME) to generate the dicarbonyl intermediate.[10] Without further isolation, the intermediates were treated with freshly sublimed Me_3NO to oxidize the carbonyl ancillaries, followed by heating in the presence of diphosphine, c.f. dppb or pp2b, to complete the carbonyl substitution. The imidazolyl derivatives with formula $[Os(ibifp)_2(dppb)]$ (**4**) and $[Os(iifp)_2(dppb)]$ (**5**) were also synthesized using similar experimental approach. Mass analyses and ^1H and ^{19}F NMR spectroscopies were conducted to provide the initial characterization data. **Scheme 3** gives the structural drawing of these Os(II) complexes.

Single crystal X-ray diffraction study on **1** was executed to reveal the general coordination structure of these Os(II) metal complexes. As can be seem in **Figure 1**, the molecule possesses a twofold rotational axis and with two btfp chromophores and a unique dppb chelate. The octahedral geometry around the central Os(II) metal is slightly distorted, as shown by the less-than-linear *trans*-N(2)-Os-N(2A) angle of 168.1(1)° for the pyrazolate fragments and *cis*-angles between the two thiazolyl fragments, c.f. N(1)-Os-N(1A) = 88.1(1)°. The overall molecular geometry is similar to those found in the relevant, group 8 bis-pyridyl azolate complexes with either diphosphine[7a] or diimine chelates.[11]

2.2. Photophysical Properties

UV/Vis spectra of the titled complexes are illustrated in **Figure 2**, while the numerical photophysical data is summarized in **Table 1**. On the basis of previous studies,[12] it is unambiguous to assign the lowest-lying absorption band with lower molar extinction coefficients (ε) to the metal-to-ligand (thiazol-2-yl or imidazol-2-yl moiety) charge transfer transition (MLCT) mixed, to certain extents, with the intra-ligand $\pi\pi^*$ excitation. Subsequently, the higher lying absorption bands in the region of 300–350 nm with ε value > 10^4 $M^{-1}cm^{-1}$ are ascribed to the intra-ligand $\pi\pi^*$ transition mainly associated with the heteroaromatic chelates.

Upon excitation, as shown in Figure 2, the titled complexes **1–3** showed bright orange to red emissions, with quantum yield (Q.Y.) > 0.1 in CH_2Cl_2 with peak wavelength ranging from 580 nm to 650 nm. Blue shifted emission with peak maximum ~538 nm was observed for **4** with much weaker emission intensity (Q.Y. ~3.2×10^{-3}), while **5** is virtually non-emissive. Table 1 summarizes the observed lifetimes together with the calculated radiative (k_r) and non-radiative (k_{nr}) rate constants. First of all, the radiative decay rate constants are derived to be ~10^5 s^{-1} for **1–4**, ascertaining their phosphorescent origin. The sulfur atom of the thiazolyl groups tends to possess the greater polarizability,[13] so that all thiazolyl Os(II) complexes **1–3** have showed much red-shifted absorption compared with their pyridyl counterparts.[12b] On the other hand, the trivalent

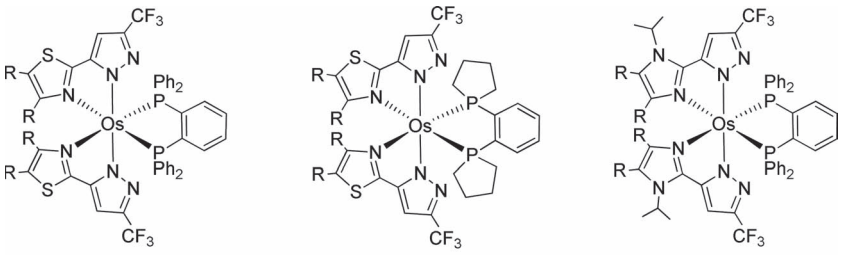

Scheme 3. Structural drawing for Os(II) complexes **1–5**.

nitrogen atom of the imidazolyl groups possess higher electron density and less polarizability, which then induces the blue-shift of both absorption and emission spectra of complex **4**. The further blue shift of the absorption for **5** (c.f. **4**) can be rationalized by the less π-conjugation due to the lack of fused benzo moiety. Despite the increase of energy gap and thus less influence of energy gap law to quench the emission,[14] the opposite result, i.e. weak and no emission, observed for **4** and **5** respectively is intriguing, which deserves in-depth probe for the possible quenching mechanism elaborated as follows.

Time-dependent DFT calculations were then performed to gain more insight into the fundamental basis. **Figure 3** depicts the selected frontier orbitals involved in the lower-lying transitions of complexes **1–5**. All pertinent energy gaps and corresponding assignments of each transition are listed in **Table 2**. The calculated energy gaps of the S_0-S_1 transition for **1**: 470.2 nm, **2**: 491.1 nm, **3**: 448.3 nm, **4**: 412.6 nm and **5**: 372.2 nm are close to the observed onsets of the absorption peaks recorded in Figure 2. Moreover, the calculated energy gaps of T_1 states for **1**: 505.6 nm, **2**: 525.2 nm, **3**: 485.4 nm, **4**: 435.9 nm, are also in agreement with the trend of the first vibronic peak of their phosphorescence spectra. This result indicates that the TDDFT calculation works well in predicting the lowest Franck-Condon excited state for both absorption and emission based on the S_0 optimized geometries of the titled complexes.

As for the absorption characteristic, frontier orbital analyses indicate that the lowest triplet excited states (T_1) for complexes **1–5** are primarily attributed to HOMO "LUMO transition (Table 2). Moreover, as depicted in Figure 3, the HOMO of complexes **1–5** are mainly localized at the central metal atom, and in small part at the azolate fragments, and the LUMO of complexes **1–5** are localized at the btfp (**1** and **2**), tfp (**3**) and ibifp (**4**) moieties, implying that the $S_0 \rightarrow T_1$ transition involves Os(II) d_π to ligand MLCT transition mixed mainly with the intra-ligand $\pi\pi^*$ charge transfer (ILCT) process. As for the phosphorescence character we then performed the geometry optimization along the triplet state potential energy surface (PES) and carefully examined the relatively energy gap between ^{3}MLCT/$\pi\pi^*$ and ^{3}MC *dd* states for complexes **1–5**. Note that the ^{3}MC *dd* state possesses a repulsive PES, which in theory will touch the ground-state PES, resulting in the dominant radiationless deactivation process.[15] In this computational approach, the energy of higher lying ^{3}MC *dd* states was calculated following the methodology illustrated in previous work.[16] Description of the calculation procedures can be seen in the experimental section.

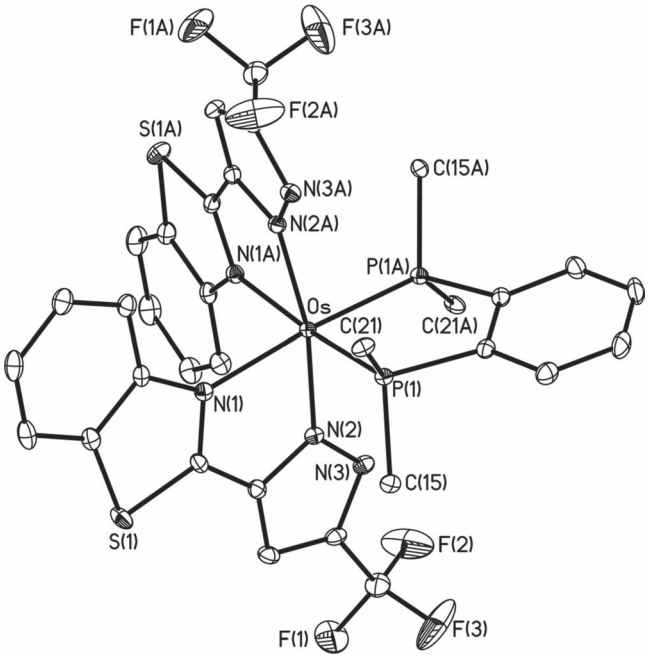

Figure 1. ORTEP diagram of Os(II) complex **1** with thermal ellipsoids shown at 30% probability level; all four phenyl groups on dppb were omitted for clarity. Selected bond distances: Os–N(1) = 2.188(3), Os–N(2) = 2.066(3) and Os–P(1) = 2.2623(8) Å; selected bond angles: N(1)-Os-P(1) = 93.81(7), N(1)-Os-P(1A) = 174.94(7), N(1)-Os-N(2) = 76.6(1), N(1)-Os-N(1A) = 88.1(1), P(1)-Os-P(1A) = 84.73(4) and N(2)-Os-N(2A) = 168.1(1)°.

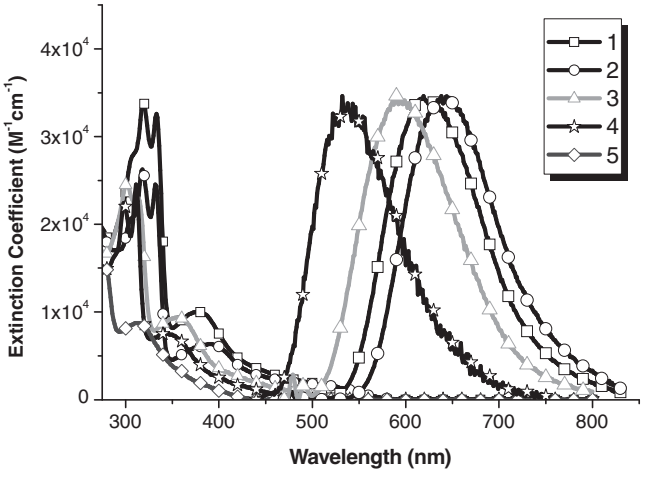

Figure 2. Absorption and normalized emission spectra of complexes **1–5** in degassed CH_2Cl_2 at RT. Note that the emission of complex **5** is too weak to be recorded.

Table 1. Selected photophysical data of Os(II) complexes **1–5** in degassed CH_2Cl_2 solution at RT.

cpd	abs. λ_{max}(nm) [$\varepsilon \times 10^{-3}$]	em. λ_{max} (nm)	Q.Y.	τ_{obs} (μs)	k_r (s^{-1})	k_{nr} (10^5 s^{-1})
1	319(34), 333(33), 379(10), 502(1.8)	622	0.49	1.77	2.77×10^5	2.88×10^5
2	318(26), 332(25), 390(6.3), 514(1.7)	642	0.65	2.58	2.52×10^5	1.36×10^5
3	302(24.6), 314(22.9), 355(9.4)	580	0.11	0.49	2.04×10^5	1.84×10^6
4	298(22.4), 311(24.5), 344(7.5)	538	0.003	0.024	1.36×10^5	4.21×10^7
5	313(8.7)	–	–	–	–	–

Comparing the state energy levels of **1** and **3** (or **4** and **5**) shown in **Figure 4**, it is noticeable that shortening the π-conjugation system increases both the ππ* and $d_\pi \rightarrow \pi^*$ MLCT gap, and hence the MLCT/ππ* energy level is in a trend of **3** > **1** and **5** > **4**. On the other hand, since the π* orbital is located at the imidazolyl group for **4** and **5**, in which the trivalent nitrogen atom is considered to be stronger electron donating group (c.f. thiazol-2-yl group in **1**–**3**), the ππ* energy is

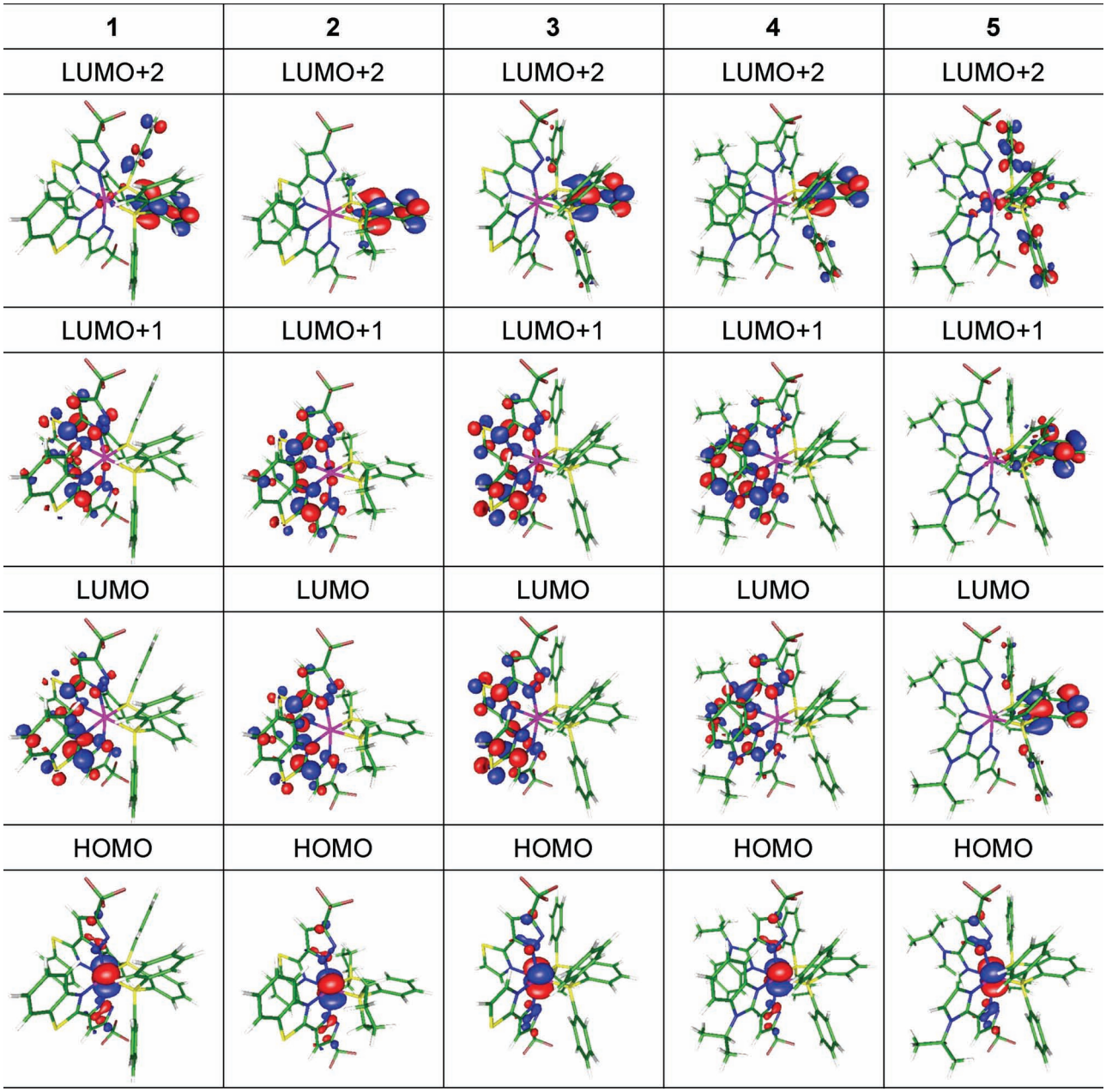

Figure 3. Selected frontier orbitals involved in the lower-lying transition for **1–5**.

Table 2. Computational energy levels, oscillator strengths and orbital transition analyses of S_1 and T_1 states for Os(II) complexes **1–5**.

cpd	States	λ_{cal} (nm)	f	Assignments	MLCT(%)
1	T_1	505.6	0	HOMO→LUMO (81%)	57.56
	S_1	470.2	0.0189	HOMO→LUMO (98%)	65.91
2	T_1	525.2	0	HOMO→LUMO (90%)	64.90
	S_1	491.1	0.023	HOMO→LUMO (99%)	67.25
3	T_1	485.4	0	HOMO→LUMO (67%)	57.23
	S_1	448.3	0.0103	HOMO→LUMO (99%)	67.27
4	T_1	435.9	0	HOMO→LUMO (71%)	48.54
	S_1	412.6	0.016	HOMO→LUMO (98%)	66.99
5	T_1	390.6	0	HOMO→LUMO+2 (70%)	46.12
	S_1	372.2	0.0001	HOMO→LUMO (99%)	67.56

accordingly raised. Likewise, both Os(II) d_π and pyrazolate π orbital will be lifted as well, but such an inductive perturbation by the trivalent nitrogen atom is indirect and hence should be less in degree than that of π^* orbital. As a result, substantial raise of the ^{3}MLCT/$\pi\pi^*$ energy is obtained for **4** and **5**.

Evidence of the above theoretical viewpoint is supported experimentally by the electrochemical data acquired for the titled complexes (see **Table 3**), in which the oxidation potential for **4** and **5** is lower than that of **1–3**, whereas the decrement is smaller than the increment of the corresponding reduction potential. Conversely, the ^{3}MC *dd* energy level of **3–5** remains relatively unchanged, shown in Figure 4. For complexes **1** and **2**, the ^{3}MC *dd* state cannot be located via current calculation. This may indicate that the ^{3}MC *dd* state is substantially higher in energy than that of the lowest lying ^{3}MLCT/$\pi\pi^*$ state, accounting for the high emission Q.Y. observed for **1** (0.49) and **2** (0.65) (see Table 1). Interestingly, the ^{3}MC *dd* state of **5** is calculated to be lower in energy than

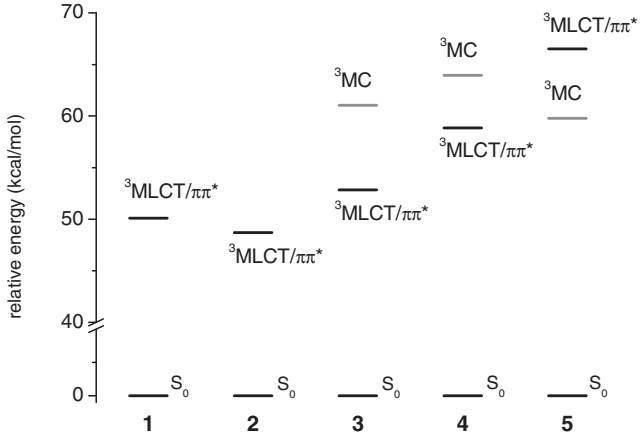

Figure 4. Energy diagram of complexes **1–5** in terms of ^{3}MC and ^{3}MLCT/$\pi\pi^*$ states, in which the ^{3}MLCT/$\pi\pi^*$ states were obtained from unrestricted optimization, the ^{3}MC *dd* state is also refined by the same method, but the initial structure is from a highly distorted molecular geometry (see text for detail).

Table 3. The electrochemical data of Os(II) complexes.[a)]

cpd	Ox. $E_{1/2}$ (ΔE_p)[b)]	Red. $E_{1/2}$ (ΔE_p)[c)]
1	0.19(83)	−2.52(120), −2.78(141)
2	0.13(81)	−2.51(119), −2.71(146)
3	0.16(84)	−2.76(105), −2.91(212)
4	−0.03(96)	−3.13(94), −3.30(101)
5	−0.10(114)	−3.27(258)

[a)]The oxidation and reduction experiments were conducted in CH_2Cl_2 and THF solution, respectively. [b)]Ox. $E_{1/2}$ refers to $[(E_{pa} + E_{pc})/2]$, in which E_{pa} and E_{pc} are the anodic and cathodic peak potentials referenced to the Fc^+/Fc couple in V, while $\Delta E_p = |E_{pa} - E_{pc}|$ was reported in mV. [c)]Red. $E_{1/2}$ refers to $[(E_{pa} + E_{pc})/2]$, in which E_{pa} and E_{pc} are the anodic and cathodic peak potentials referenced to the Fc^+/Fc couple in V, while $\Delta E_p = |E_{pa} - E_{pc}|$ was reported in mV.

that of the ^{3}MLCT/$\pi\pi^*$ state. The result predicts the occurrence of dominant radiationless quenching process from the ^{3}MC *dd* state, consistent with the lack of emission observed experimentally. As for complex **4**, due to the relatively small energy gap between ^{3}MC *dd* and ^{3}MLCT/$\pi\pi^*$ states, thermal population (from ^{3}MLCT/$\pi\pi^*$) to the ^{3}MC *dd* state is possible, giving the weak emission. Such a quenching process may be activated through certain vibronic modes associated with the elongation of the metal-ligand bond distance, which can be suppressed, in part, via forming the rigid solid crystal or film,[17] as evidenced by the enhanced emission Q.Y. of **4** acquired in the solid film (vide infra).

2.3 Thin-Film Photophysics and OLED Characteristics

The fabrication of OLED was mainly divided into two techniques; i.e. vacuum deposition[18] and solution process.[19] Although multi-layered architecture with excellent efficiency can be achieved by vacuum deposition, its downside is the complexities, especially for deposition of emission layers (EMLs), in which hosts and dopants of various ratios need to be mixed in a homogeneous manner. On the other hand, the solution process is mature for depositing thin films with efficient material utilization and without complex multi-component co-evaporation process. The remaining challenge is to design dopants and host materials for achieving adequate solubility and high homogeneity, and high emission Q.Y. in solid-state matrices.

Accordingly, a series of solution-processed OLEDs using aforementioned Os(II) dopants **1–4** in 4,4′,4″-Tris(N-carbazolyl)-triphenylamine (TCTA) matrix as EMLs were fabricated, for which their photophysical properties are listed in **Table 4**. It is notable that the EML thin films of **1–3** show promising Q.Y.s of

Table 4. Photophysical properties of the dopant: TCTA thin-film for complexes **1–4.**

cpd	Q.Y.	τ_{obs} (μs)	k_r (s^{-1})	k_{nr} (s^{-1})
1	0.87	2.04	4.26×10^5	6.37×10^4
2	0.65	2.10	3.10×10^5	1.67×10^5
3	0.80	1.15	6.96×10^5	1.74×10^5
4	0.50	1.17	4.27×10^5	4.27×10^5

over 60%, among which the orange-red emission **2** even show the highest Q.Y. of 85%. These results are also supported by prolonged and mono-exponential-decay of transient photoluminescence (PL) measurement, confirming the high homogeneity and luminescence of thin films. As showed in Table 4, the nonradiative decay rate of these Os(II) phosphors turns much smaller in thin film than in fluid solution listed in Table 1, and giving a nearly double digit increase in emission Q.Y. for the benzimidazolyl complex **4**. It is believed that, upon excitation in the fluid solution, the phosphor can undergo geometrical distortions such as bond elongations or torsional distortions away from the ground state geometry. This can lead to a stabilization of the metal *dd* excited state(s) and consequently increase their thermal population. However, in a more "rigid" environment, like in the TCTA host matrix, relevant structural distortions or related energy stabilizations of the quenching states are largely prevented or are at least less distinct, showing the observed increase in emission efficiencies.[17] Moreover, the EL spectra are shown in **Figure 5**, for which the benzothiazolyl dopants **1**, **2** and **3** exhibit orange-red emission with peak wavelength located at 608 nm, 620 nm and 582 nm, respectively, while benzimidazolyl phosphors **4** exhibit green emission centered at 518 nm. Moreover, the schematic device structure and the energy level diagram of each component are also showed in Figure 5. As can be seen, the HOMO of TCTA is about 5.7 eV, which is much greater than the HOMO of all Os(II) emitters, such that the dominant mechanism for forming excitons in the present system is through direct charge carrier trapping and recombination.[20]

Current efficiency-luminance characteristics of these devices are shown in **Figure 6**a. The orange-red phosphors **1**, **2** and **3** show impressive maximum current efficiencies of 31.1 $cd \cdot A^{-1}$, 18.3 $cd \cdot A^{-1}$ and 42.1 $cd \cdot A^{-1}$, respectively. Green-emitting dopant **4** also achieved remarkably high maximum current efficiency of 48.3 $cd \cdot A^{-1}$. All devices show sufficiently low turn-on voltage of ~2.6 V, and the performances are among the highest ever reported in solution processed OLEDs and even comparable to the literature reports based on the state-of-the-art vacuum deposition and with more complicated device structures.[18a,18b,21]

Figure 6b shows the external quantum efficiencies (EQEs), for which the max. EQE are recorded to be 17.7% (**1**), 15.6% (**2**), 15.7% (**3**) and 15.6% (**4**), respectively. If we assume 25% out-coupling ratio for regular bottom-emission OLEDs,[22] the EQE values are closed to the out-coupling efficiency multiply by the Q.Y.s of the EMLs. The result clearly indicates that good carriers balance has been achieved in these solution based devices without additional losses after generation of photons from EMLs, except for coupling of the unescape (waveguiding and surface-plasmon) modes inside the layer structures. The device characteristics of OLEDs are summarized in **Table 5**. It is notable that the benzothiazolyl Os(II) complexes **1** and **3** with dppb chelate have showed better photo- and electro- luminescence than that of their pp2b counterpart **2**, a result attributed to the more rigid phenyl ancillaries of dppb versus that of the tetramethylene entities of pp2b. This observation is in good agreement with the recent report on the bulky substituents[23] that render several advantages: i) the improvement of microscopic dispersion between the host and dopant and/or ii) the inhibition or reduction of back energy transfer due to their increased spatial separation between dopant and host molecules in EML, leading to superior device performance.

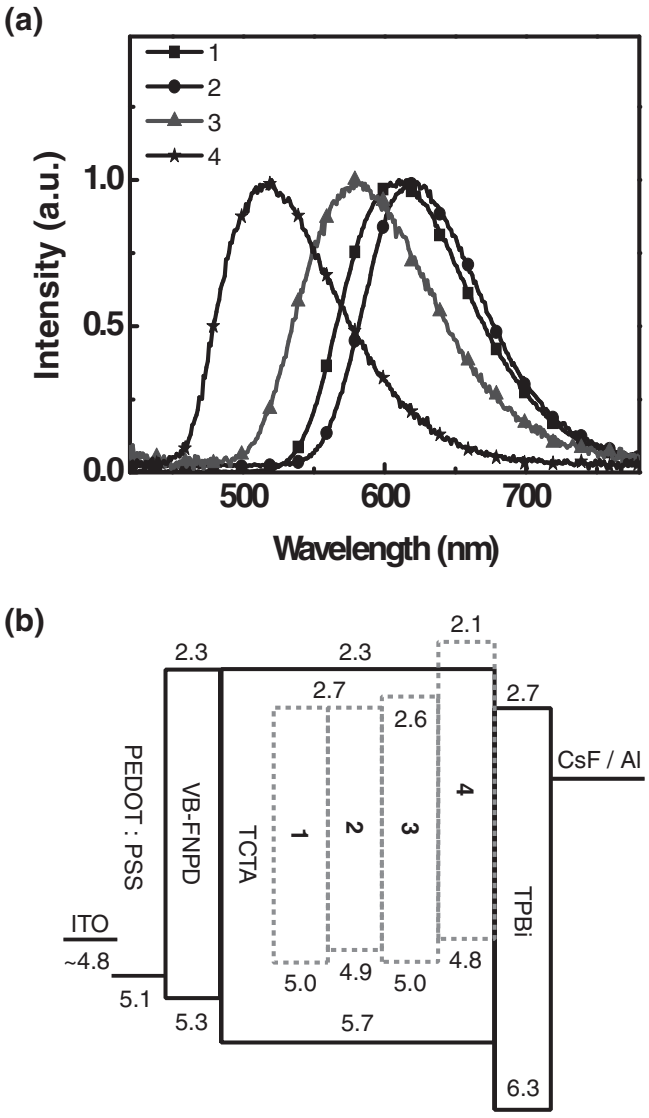

Figure 5. (a) Electroluminescence and (b) energy level diagram of each material reported in this study.

3. Conclusion

In summary, by judicious molecular design, novel Os(II) complexes which show bright emission spanning region from green to saturated red have been synthesized. Highly efficient solution-processed small-molecule OLEDs based on these complexes were demonstrated. Low driving voltages, high EQEs and high EL efficiencies up to (31.1 $cd \cdot A^{-1}$, 34.1 $lm \cdot W^{-1}$) and (42.1 $cd \cdot A^{-1}$, 47.2 $lm \cdot W^{-1}$) were achieved in red and orange OLEDs, respectively. The efficiency values are among the highest performance of solution-processed phosphorescent OLEDs

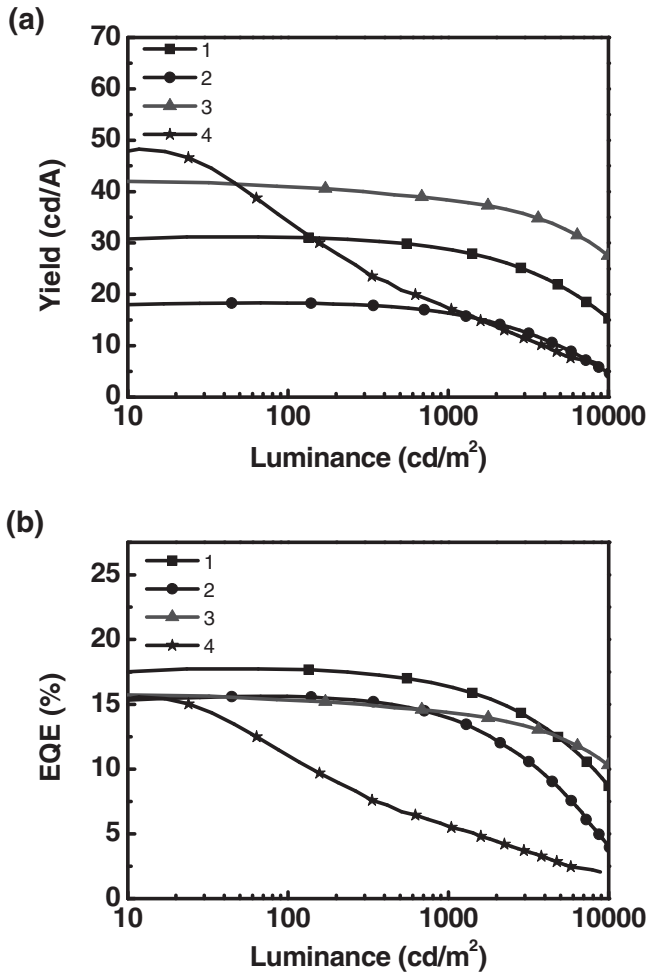

Figure 6. (a) Current efficiency and (b) external quantum efficiency characteristics versus to luminance of solution processed OLEDs.

reported to date. Successful attempt to push Os(II) based emission into green region has become possible upon employment of benzimidazolyl chromophore. OLEDs utilizing this green emitting Os(II) complex also shows high current and power efficiencies (48.3 $cd \cdot A^{-1}$, 50.9 $lm \cdot W^{-1}$). These encouraging results imply that these Os(II) phosphors should be promising green to saturated red emitters for high-efficiency and low-cost solution processable OLEDs. It is worthy to note that complex **4** is the only Os(II) based phosphor so far suitable for the fabrication of highly efficient green-emitting OLEDs.

4. Experimental Section

General Procedures: All reactions were performed under argon atmosphere and solvents were distilled from appropriate drying agents prior to use. Commercially available reagents were used without further purification unless otherwise stated. The 2-bis(phospholano) benzene (pp2b) chelate [24], as well as the functionalized pyrazole [9], i.e. 5-(benzothiazol-2-yl)-3-trifluoromethylpyrazole (btfpH), 5-(thiazol-2-yl)-3-trifluoromethylpyrazole (tfpH), 5-(1-isopropylbenzimidazol-2-yl)-3-trifluoromethylpyrazole (ibifpH) and 5-(1-isopropylimidazol-2-yl)-3-trifluoromethylpyrazole (iifpH), were synthesized according to the literature procedures. All synthetic manipulation was monitored using pre-coated TLC plates (0.20 mm with fluorescent indicator UV254). Mass spectra were obtained on a JEOL SX-102A instrument operating in electron impact (EI) or fast atom bombardment (FAB) mode. All NMR spectra were recorded on a Varian INOVA-500 instrument. Elemental analysis was carried out with a Heraeus CHN-O Rapid Elementary Analyzer. Cyclic voltammetry (CV) measurements were performed using a BAS 100 B/W electrochemical analyzer.

Preparation of [Os(btfp)$_2$(dppb)]: A mixture of $Os_3(CO)_{12}$ (200 mg, 0.22 mmol) and 5-(benzothiazol-2-yl)-3-trifluoromethylpyrazole (btfpH, 374 mg, 1.39 mmol) in diethylene glycol monomethyl ether (DGME, 30 mL) was heated to reflux for 24 hr. After cooling to RT, the freshly sublimed Me_3NO (104 mg, 1.39 mmol) in DGME (10 mL) was added dropwise into the aforementioned mixture and refluxed for another 1 hr at 110 °C. After cooling to RT, 1,2-bis(diphenylphosphino)benzene (dppb, 310 mg, 0.70 mmol) was added and heated for 24 hr at 190 °C. Finally, the solvent was removed under vacuum and the residue was purified by column chromatography over silica gel eluting with a 1:4 mixture of ethyl acetate and hexane, followed by recrystallization from a mixture of CH_2Cl_2 and methanol at RT, giving red-orange crystalline solid (**1**, 509 mg, 0.43 mmol, 66%).

Spectral data of **1**: ^{1}H NMR (400 MHz, d_6-acetone, 294K, δ): 7.83 ~ 7.73 (m, 8H), 7.58 ~ 7.55 (m, 2H), 7.20 (t, J = 7.6 Hz, 4H), 7.11 ~ 7.05 (m, 6H), 6.91 (td, J = 7.8, 1.2 Hz, 2H), 6.85 ~ 6.78 (m, 6H), 6.69 (t, J = 8.4 Hz, 4H), 5.71 (d, J = 8.4 Hz, 2H); ^{19}F–{^{1}H} NMR (470 MHz, d_6-acetone, 294K, δ): –61.28 (s, 6F); ^{31}P–{^{1}H} NMR (202 MHz, d_6-acetone, 294K, δ): 29.34 (s, 2P); MS (FAB, ^{192}Os): m/z 1174 [M]$^+$. Anal. calcd for $C_{52}H_{34}F_6N_6OsP_2S_2$: C 53.24, H 2.92, N 7.16; found: C 53.02, H 3.17, N 7.26.

Selected crystal data of **1**: $C_{53}H_{36}Cl_2F_6N_6OsP_2S_2$; M = 1258.04; orthorhombic; space group = P bcn; a = 17.3907(10) Å, b = 15.5879(8) Å, c = 17.7782(10) Å, V = 4819.4(5) Å^3; Z = 4; ρ_{calcd} = 1.734 $Mg \cdot m^{-3}$; $F(000)$ = 2488; crystal size = 0.36 × 0.20 × 0.20 mm^3; λ(Mo-K_α) = 0.71073 Å; T = 150(2) K; μ = 2.980 mm^{-1}; 25404 reflections collected, 5548 independent reflections (R_{int} = 0.0467), data/ restraints/ parameters = 5548/ 0/ 326; GOF = 1.018, final $R_1[I > 2\sigma(I)]$ = 0.0304 and wR_2 (all data) = 0.0694. The crystallographic data (excluding structure factors) has been deposited in the Cambridge Crystallographic Data Centre with the deposition number CCDC-876195. This data can be obtained free of charge on application to CCDC, 12 Union Road, Cambridge CB21EZ, UK (fax: (+44) 1223-336-033; e-mail: deposit@ccdc.cam.ac.uk).

Preparation of [Os(btfp)$_2$(pp2b)]: Similar to that reported for **1**, red crystalline solid of Os(btfp)$_2$(pp2b) (**2**) was obtained from sequential reaction of $Os_3(CO)_{12}$ with 5-(benzothiazol-2-yl)-3-trifluoromethylpyrazole

Table 5. The performance data of OLEDs in this work.

	1	2	3	4
Turn on voltage (V) (0.1 cd/m^2)	2.6	2.7	2.5	2.5
Current efficiency (cd/A) (max, 100 cd/m^2)	31.1, 31.1	18.3, 18.3	42.1, 41.0	48.3, 34.2
Power efficiency (lm/W) (max, 100 cd/m^2)	34.1, 29.5	17.6, 13.0	47.2, 39.6	50.9, 22.2
CIE (x, y)	(0.58, 0.41)	(0.63, 0.37)	(0.49, 0.48)	(0.30, 0.53)
EQE (%) (max, 100 cd/m^2)	17.7, 17.7	15.6, 15.6	15.7, 15.4	15.6, 11.0

(btfpH), followed by addition of Me_3NO and then 2-bis(phospholano) benzene (pp2b). Yield: 67%.

Spectral data of **2**: ^{1}H NMR (400 MHz, d_6-acetone, 294K, δ): 7.99 (d, J = 7.6 Hz, 2H), 7.85 ~ 7.81 (m, 2H), 7.51 ~ 7.48 (m, 2H), 7.37 ~ 7.33 (m, 4H), 7.20 ~ 7.16 (m, 2H), 6.18 (d, J = 8.4 Hz, 2H), 3.19 ~ 3.12 (m, 2H), 2.51 ~ 2.45 (m, 2H), 1.88 ~ 1.72 (m, 4H), 1.30 ~ 1.24 (m, 2H), 1.17 ~ 1.11 (m, 2H), 0.96 ~ 0.90 (m, 2H), 0.79 ~ 0.72 (m, 2H); ^{19}F–{^{1}H} NMR (376 MHz, d_6-acetone, 294K, δ): –60.58 (s, 6F); ^{31}P–{^{1}H} NMR (202 MHz, d_6-acetone, 294K, δ): 39.32 (s, 2P); MS (FAB, ^{192}Os): m/z 978 $[M]^+$. Anal. calcd for $C_{36}H_{30}F_6N_6OsP_2S_2$: C 44.26, H 3.10, N 8.60; found: C 44.49, H 3.34, N 8.69.

Preparation of [Os(tfp)$_2$(dppb)]: Similar to that reported for **1**, orange-yellow solid of [Os(tfp)$_2$(dppb)] (**3**) was obtained from sequential reaction of $Os_3(CO)_{12}$ with 5-(thiazol-2-yl)-3-trifluoromethylpyrazole (tfpH), followed by addition of Me_3NO and then 1,2-bis(diphenylphosphino) benzene (dppb). Yield: 72%.

Spectral data of **3:** ^{1}H NMR (400 MHz, d_6-acetone, 294K, δ): 7.99 ~ 7.94 (m, 4H), 7.71 ~ 7.67 (m, 2H), 7.47 ~ 7.45 (m, 2H), 7.34 (td, J = 7.4, 1.2 Hz, 2H), 7.29 (d, J = 3.2 Hz, 2H), 7.23 (td, J = 7.6, 2.0 Hz, 4H), 7.11 (td, J = 7.4, 1.2 Hz, 2H), 6.85 (td, J = 7.6, 1.6 Hz, 4H), 6.76 (s, 2H), 6.60 (t, J = 9.0 Hz, 4H), 6.26 (d, J = 3.6 Hz, 2H); ^{19}F–{^{1}H} NMR (376 MHz, d_6-acetone, 294K, δ): –60.70 (s, 6F); ^{31}P–{^{1}H} NMR (202 MHz, d_6-acetone, 294K, δ): 29.52 (s, 2P); MS (FAB, ^{192}Os): m/z 1075 $[M+1]^+$. Anal. calcd for $C_{44}H_{30}F_6N_6OsP_2S_2$: C 49.25, H 2.82, N 7.83; found: C 48.86, H 3.07, N 7.77.

Preparation of [Os(ibifp)$_2$(dppb)]: Similar to that reported for **1**, yellow solid of [Os(ibifp)$_2$(dppb)] (**4**) was obtained from sequential reaction of $Os_3(CO)_{12}$ with 5-(1-isopropylbenzimidazol-2-yl)-3-trifluoromethylpyrazole (ibifpH), followed by addition of Me_3NO and then dppb. Yield: 49%.

Spectral data of **4**: ^{1}H NMR (400 MHz, d_6-acetone, 294K, δ): 7.84 ~ 7.79 (m, 4H), 7.71 ~ 7.66 (m, 2H), 7.50 ~ 7.46 (m, 4H), 7.17 (td, J = 7.4, 1.2 Hz, 2H), 7.07 ~ 6.98 (m, 8H), 6.82 (s, 2H), 6.78 ~ 6.70 (m, 6H), 6.65 ~ 6.61 (m, 4H), 5.50 (d, J = 8.4 Hz, 2H), 5.01 (sept, J = 6.8 Hz, 2H), 1.53 (d, J = 6.8 Hz, 6H), 1.32 (d, J = 6.8 Hz, 6H); ^{19}F–{^{1}H} NMR (376 MHz, d_6-acetone, 294K, δ): –60.39 (s, 6F); ^{31}P–{^{1}H} NMR (202 MHz, d_6-acetone, 294K, δ): 31.65 (s, 2P); MS (FAB, ^{192}Os): m/z 1225 $[M+1]^+$. Anal. calcd for $C_{58}H_{48}F_6N_8OsP_2$: C 56.95, H 3.96, N 9.16; found: C 56.89, H 4.24, N 8.99.

Preparation of [Os(iifp)$_2$(dppb)]: Similar to that reported for **1**, pale yellow solid of [Os(iifp)$_2$(dppb)] (**5**) was obtained from sequential reaction of $Os_3(CO)_{12}$ with 5-(1-isopropylimidazol-2-yl)-3-trifluoromethylpyrazole (iifpH), followed by addition of Me_3NO and then dppb. Yield: 16%.

Spectral data of **5:** ^{1}H NMR (400 MHz, d_6-acetone, 294K, δ): 8.00 (t, J = 8.8 Hz, 4H), 7.63 (m, 2H), 7.38 ~ 7.35 (m, 2H), 7.30 (t, J = 7.2 Hz, 2H), 7.21 (t, J = 7.4 Hz, 4H), 7.03 (t, J = 7.2 Hz, 2H), 6.92 (d, J = 1.2 Hz, 2H), 6.80 (t, J = 7.2 Hz, 4H), 6.58 (t, J = 8.6 Hz, 4H), 6.52 (s, 2H), 5.72 (d, J = 1.2 Hz, 2H), 4.59 (sept, J = 6.8 Hz, 2H), 1.33 (d, J = 6.6 Hz, 6H), 1.31 (d, J = 6.6 Hz, 6H); ^{19}F–{^{1}H} NMR (376 MHz, d_6-acetone, 294K, δ): –60.17 (s, 6F); ^{31}P–{^{1}H} NMR (202 MHz, d-acetone, 294K, δ): 30.81 (s, 2P); MS (FAB, ^{192}Os): m/z 1124 $[M]^+$. Anal. calcd for $C_{50}H_{44}F_6N_8OsP_2$: C 53.47, H 3.95, N 9.98; found: C 53.17, H 4.12, N 9.83.

Single Crystal X-Ray Diffraction Studies: Single crystal X-ray diffraction data were measured with a Bruker SMART Apex CCD diffractometer using (Mo-K_α) radiation (λ = 0.71073 Å). The data collection was executed using the SMART program. Cell refinement and data reduction were performed with the SAINT program. The structure was determined using the SHELXTL/PC program and refined using full-matrix least squares.

Device Fabrication: Indium tin oxide (ITO) coated glass substrates (sheet resistance ~10 Ω/sq) were cleaned in an ultrasonic bath with de-ionized water, acetone, and methanol for 15 min, respectively. The glasses substrates were then treated by UV-ozone. The PEDOT:PSS (poly(3,4-ethylenedioxythiophene):poly(styrene sulfonate)) (~40 nm, measured by spectroscopic ellipsometer) was spin coated onto the substrates. The PEDOT:PSS films were then dried in air at 135 °C for 30 min. Solution of VB-FNPD (10 mg·mL^{-1}) was prepared using chlorobenzene as solvent, and the VB-FNPD films were then spin-coated onto the PEDOT:PSS/ITO substrates.[25] The samples were then baked on a hot plate at 100 °C for 30 min to remove the solvent and then 230 °C for 90 min for crosslinking. Os(II) complexes, i.e. **1–4** were doped individually in the TCTA matrix as emission layer which was spin-coated onto the VB-FNPD layer. The samples were baked again at 80 °C for 30 min to remove residual solvent. The electron transporting layer (ETL) TPBi (2,2′,2″-(1,3,5-phenylene)tris(1-phenyl-1H-benzimidazole)) and cesium fluoride/aluminum (CsF/Al) cathode were next deposited under vacuum with base pressure ~ 10^{-6} Torr. All of the subsequent processes were done in inert atmosphere without exposure to air. The device structures are: ITO (150 nm)/PEDOT:PSS (40 nm)/VB-FNPD (30 nm)/TCTA:dopant (10 wt%, 20 nm)/TPBi (50 nm)/CsF (1 nm)/Al (150 nm) for complexes **1–3** and ITO (150 nm)/PEDOT:PSS (40 nm)/VB-FNPD (30 nm)/TCTA:dopant (10 wt%, 20 nm)/TPBi (70 nm)/CsF (1 nm)/Al (150 nm) for complex **4**. The active area of the device was 1 mm^2. All measurements were conducted in glove box filled with inert gas.

Device and Thin-film Characterization: The current-voltage-luminance characteristics of OLEDs were measured by Keithley 2636A Source meter and silicon photodetector calibrated with Photo Research, Inc. PR-650 SpectraScan Colorimeter. The electroluminescence (EL) spectra were taken using a calibrated CCD spectragraph. The thicknesses of organic films were acquired with a V-VASE variable-angle spectroscopic ellipsometer (J. A. Woollam Inc.). Absolute quantum yields (Q.Y.s) of organic films were obtained using an integrating sphere (Labsphere) system integrated with a thermoelectric cooling CCD spectragraph. Time resolved photo-luminescence was measured using Multi-Channel Scaling (MCS) single photon counting system equipped with red-enhanced thermoelectric cooling photomultiplier (Becker & Hickl).

Computational Methodology: Calculation on electronic singlet and triplet states of complexes **1–5** was carried out following the methods described in our previous report.[26] In brief, the density functional theory (DFT) with B3LYP hybrid functional was applied for the computation. Time-dependent DFT (TDDFT) calculations using the B3LYP functional were then performed based on the optimized structures at ground states in combination with polarizable continuum model in dichloromethane, implemented in Gaussian 09. In this approach, restricted and unrestricted formalisms were adopted in the singlet and triplet geometry optimization, respectively. A ''double-z'' quality basis set consisting of Hay and Wadt's effective core potentials was employed for Os atom,[27] in which the relativistic effective core potential was used for the inner core electrons, leaving the outer core ($5s^25p^6$) electrons and the $5d^5$ valence electrons to be concerned.

The electronic configurations of ^{3}MC *dd* states were calculated following the literature methodology.[16] In brief, the ^{3}MLCT state geometry was obtained by performing geometry optimization along the triplet state potential energy surface (PES), using the core arrangement derived from the X-ray structural data of **1** as the initial geometry. As for the ^{3}MC state, because the electron densities are mainly distributed on the central metal atom, the calculation is starting with a distorted geometry, for which the metal-ligand bondings are largely elongated, such that its associated energy is expected to be far away from the global minimum along the PES, and then the geometry optimization is performed. Accordingly, the optimization is able to fall into the presumably shallow local minimum associated with the ^{3}MC *dd* excited state.

Acknowledgements

This work was supported by the National Science Council and Ministry of Economy of Taiwan, project number (100-EC-17-A-08-S1-042). We are also grateful to the National Center for High-Performance Computing for computer time and facilities.

Received: March 14, 2012
Published online: May 11, 2012

[1] a) H. Sasabe, J. Kido, *Chem. Mater.* **2011**, *23*, 621; b) L. Duan, L. Hou, T.-W. Lee, J. Qiao, D. Zhang, G. Dong, L. Wang, Y. Qiu, *J. Mater. Chem.* **2010**, *20*, 6392; c) Y. Chi, P.-T. Chou, *Chem. Soc. Rev.* **2010**, *39*, 638; d) G. Zhou, W.-Y. Wong, S. Suo, *J. Photochem. Photobio. C* **2010**, *11*, 133; e) Y. You, S. Y. Park, *Dalton Trans.* **2009**, 1267; f) W.-Y. Wong, C.-L. Ho, *Coord. Chem. Rev.* **2009**, *253*, 1709; g) C. Ulbricht, B. Beyer, C. Friebe, A. Winter, U. S. Schubert, *Adv. Mater.* **2009**, *21*, 4418; h) W.-Y. Wong, C.-L. Ho, *J. Mater. Chem.* **2009**, *19*, 4457; i) J. A. G. Williams, A. J. Wilkinson, V. L. Whittle, *Dalton Trans.* **2008**, 2081; j) P.-T. Chou, Y. Chi, *Chem. Eur. J.* **2007**, *13*, 380.

[2] a) F.-M. Hwang, H.-Y. Chen, P.-S. Chen, C.-S. Liu, Y. Chi, C.-F. Shu, F.-I. Wu, P.-T. Chou, S.-M. Peng, G.-H. Lee, *Inorg. Chem.* **2005**, *44*, 1344; b) M. K. Nazeeruddin, M. Gratzel, *Struct. Bond.* **2007**, *123*, 113; c) G. Zhou, C.-L. Ho, W.-Y. Wong, Q. Wang, D. Ma, L. Wang, Z. Lin, T. B. Marder, A. Beeby, *Adv. Funct. Mater.* **2008**, *18*, 499; d) G.-J. Zhou, Q. Wang, W.-Y. Wong, D. Ma, L. Wang, Z. Lin, *J. Mater. Chem.* **2009**, *19*, 1872; e) C.-L. Ho, Q. Wang, C.-S. Lam, W.-Y. Wong, D. Ma, L. Wang, Z.-Q. Gao, C.-H. Chen, K.-W. Cheah, Z. Lin, *Chem. Asian J.* **2009**, *4*, 89; f) G. Zhou, Q. Wang, X. Wang, C.-L. Ho, W.-Y. Wong, D. Ma, L. Wang, Z. Lin, *J. Mater. Chem.* **2010**, *20*, 7472; g) G. Zhou, W.-Y. Wong, X. Yang, *Chem. Asian J.* **2011**, *6*, 1706; h) H. Fu, Y.-M. Cheng, P.-T. Chou, Y. Chi, *Mater. Today* **2011**, *14*, 472; i) C.-L. Ho, L.-C. Chi, W.-Y. Hung, W.-J. Chen, Y.-C. Lin, H. Wu, E. Mondal, G.-J. Zhou, K.-T. Wong, W.-Y. Wong, *J. Mater. Chem.* **2012**, *22*, 215.

[3] a) S. Sprouse, K. A. King, P. J. Spellane, R. J. Watts, *J. Am. Chem. Soc.* **1984**, *106*, 6647; b) M. G. Colombo, T. C. Brunold, T. Riedener, H. U. Guedel, M. Fortsch, H.-B. Buergi, *Inorg. Chem.* **1994**, *33*, 545.

[4] A. Tsuboyama, H. Iwawaki, M. Furugori, T. Mukaide, J. Kamatani, S. Igawa, T. Moriyama, S. Miura, T. Takiguchi, S. Okada, M. Hoshino, K. Ueno, *J. Am. Chem. Soc.* **2003**, *125*, 12971.

[5] a) R. J. Holmes, S. R. Forrest, Y.-J. Tung, R. C. Kwong, J. J. Brown, S. Garon, M. E. Thompson, *Appl. Phys. Lett.* **2003**, *82*, 2422; b) J. Li, P. I. Djurovich, B. D. Alleyne, I. Tsyba, N. N. Ho, R. Bau, M. E. Thompson, *Polyhedron* **2004**, *23*, 419; c) S.-H. Eom, Y. Zheng, N. Chopra, J. Lee, F. So, J. Xue, *Appl. Phys. Lett.* **2008**, *93*, 133309; d) S.-J. Yeh, M.-F. Wu, C.-T. Chen, Y.-H. Song, Y. Chi, M.-H. Ho, S.-F. Hsu, C. H. Chen, *Adv. Mater.* **2005**, *17*, 285; e) C.-H. Yang, Y.-M. Cheng, Y. Chi, C.-J. Hsu, F.-C. Fang, K.-T. Wong, P.-T. Chou, C.-H. Chang, M.-H. Tsai, C.-C. Wu, *Angew. Chem. Int. Ed.* **2007**, *46*, 2418; f) Y.-C. Chiu, J.-Y. Hung, Y. Chi, C.-C. Chen, C.-H. Chang, C.-C. Wu, Y.-M. Cheng, Y.-C. Yu, G.-H. Lee, P.-T. Chou, *Adv. Mater.* **2009**, *21*, 2221.

[6] a) P.-T. Chou, Y. Chi, *Eur. J. Inorg. Chem.* **2006**, 3319; b) Y. Chi, P.-T. Chou, *Chem. Soc. Rev.* **2007**, *36*, 1421.

[7] a) Y.-M. Cheng, G.-H. Lee, P.-T. Chou, L.-S. Chen, Y. Chi, C.-H. Yang, Y.-H. Song, S.-Y. Chang, P.-I. Shih, C.-F. Shu, *Adv. Funct. Mater.* **2008**, *18*, 183; b) T.-C. Lee, J.-Y. Hung, Y. Chi, Y.-M. Cheng, G.-H. Lee, P.-T. Chou, C.-C. Chen, C.-H. Chang, C.-C. Wu, *Adv. Funct. Mater.* **2009**, *19*, 2639.

[8] Y.-L. Tung, P.-C. Wu, C.-S. Liu, Y. Chi, J.-K. Yu, Y.-H. Hu, P.-T. Chou, S.-M. Peng, G.-H. Lee, Y. Tao, A. J. Carty, C.-F. Shu, F.-I. Wu, *Organometallics* **2004**, *23*, 3745.

[9] a) H. Chikashita, M. Ishibaba, K. Ori, K. Ito, *Bull. Chem. Soc. Jpn* **1988**, *61*, 3637; b) S. P. Singh, D. Kumar, B. G. Jones, M. D. Threadgill, *J. Fluorine Chem.* **1999**, *94*, 199.

[10] a) P.-C. Wu, J.-K. Yu, Y.-H. Song, Y. Chi, P.-T. Chou, S.-M. Peng, G.-H. Lee, *Organometallics* **2003**, *22*, 4938; b) J.-K. Yu, Y.-H. Hu, Y.-M. Cheng, P.-T. Chou, S.-M. Peng, G.-H. Lee, A. J. Carty, Y.-L. Tung, S.-W. Lee, Y. Chi, C.-S. Liu, *Chem. Eur. J.* **2004**, *10*, 6255.

[11] K.-L. Wu, H.-C. Hsu, K. Chen, Y. Chi, M.-W. Chung, W.-H. Liu, P.-T. Chou, *Chem. Commun.* **2010**, *46*, 5124.

[12] a) M. Li, H. Zeng, Y. Meng, H. Sun, S. Liu, Z. Lu, Y. Huang, X. Pu, *Dalton Trans.* **2011**, *40*, 7153; b) Y.-L. Tung, S.-W. Lee, Y. Chi, Y.-T. Tao, C.-H. Chien, Y.-M. Cheng, P.-T. Chou, S.-M. Peng, C.-S. Liu, *J. Mater. Chem.* **2005**, *15*, 460.

[13] a) R. Wang, D. Liu, H. Ren, T. Zhang, X. Wang, J. Li, *J. Mater. Chem.* **2011**, *21*, 15494; b) J. Kuwabara, T. Namekawa, M.-a. Haga, T. Kanbara, *Dalton Trans.* **2012**, *41*, 44.

[14] J. V. Caspar, E. M. Kober, B. P. Sullivan, T. J. Meyer, *J. Am. Chem. Soc.* **1982**, *104*, 630.

[15] a) T. Sajoto, P. I. Djurovich, A. B. Tamayo, J. Oxgaard, W. A. Goddard, M. E. Thompson, *J. Am. Chem. Soc.* **2009**, *131*, 9813; b) P.-T. Chou, Y. Chi, M.-W. Chung, C.-C. Lin, *Coord. Chem. Rev.* **2011**, *255*, 2653.

[16] M. Abrahamsson, M. J. Lundqvist, H. Wolpher, O. Johansson, L. Eriksson, J. Bergquist, T. Rasmussen, H.-C. Becker, L. Hammarstroem, P.-O. Norrby, B. Akermark, P. Persson, *Inorg. Chem.* **2008**, *47*, 3540.

[17] A. F. Rausch, L. Murphy, J. A. G. Williams, H. Yersin, *Inorg. Chem.* **2012**, *51*, 312.

[18] a) C.-L. Ho, W.-Y. Wong, Q. Wang, D. Ma, L. Wang, Z. Lin, *Adv. Funct. Mater.* **2008**, *18*, 928; b) W. S. Jeon, T. J. Park, K. H. Kim, R. Pode, J. Jang, J. H. Kwon, *Org. Electron.* **2010**, *11*, 179; c) J.-Y. Hung, C.-H. Lin, Y. Chi, M.-W. Chung, Y.-J. Chen, G.-H. Lee, P.-T. Chou, C.-C. Chen, C.-C. Wu, *J. Mater. Chem.* **2010**, *20*, 7682.

[19] a) F. So, B. Krummacher, M. K. Mathai, D. Poplavskyy, S. A. Choulis, V.-E. Choong, *J. Appl. Phys.* **2007**, *102*, 091101; b) C.-H. Chien, S.-F. Liao, C.-H. Wu, C.-F. Shu, S.-Y. Chang, Y. Chi, P.-T. Chou, C.-H. Lai, *Adv. Funct. Mater.* **2008**, *18*, 1430; c) S. Ye, Y. Liu, K. Lu, W. Wu, C. Du, Y. Liu, H. Liu, T. Wu, G. Yu, *Adv. Funct. Mater.* **2010**, *20*, 3125; d) T. Earmme, E. Ahmed, S. A. Jenekhe, *Adv. Mater.* **2010**, *22*, 4744; e) X.-H. Zhu, J. Peng, Y. Cao, J. Roncali, *Chem. Soc. Rev.* **2011**, *40*, 3509; f) R. Wang, D. Liu, R. Zhang, L. Deng, J. Li, *J. Mater. Chem.* **2012**, *22*, 1411.

[20] a) F.-I. Wu, P.-I. Shih, C.-F. Shu, Y.-L. Tung, Y. Chi, *Macromolecules* **2005**, *38*, 9028; b) Y.-H. Niu, M. S. Liu, J.-W. Ka, J. Bardeker, M. T. Zin, R. Schofield, Y. Chi, A. K.-Y. Jen, *Adv. Mater.* **2007**, *19*, 300.

[21] M.-T. Lee, M.-T. Chu, J.-S. Lin, M.-R. Tseng, *J. Phys. D: Appl. Phys.* **2010**, *43*, 442003.

[22] C. Adachi, M. A. Baldo, M. E. Thompson, S. R. Forrest, *J. Appl. Phys.* **2001**, *90*, 5048.

[23] a) S. M. King, H. A. Al-Attar, R. J. Evans, A. Congreve, A. Beeby, A. P. Monkman, *Adv. Funct. Mater.* **2006**, *16*, 1043; b) M. Mydlak, M. Mauro, F. Polo, M. Felicetti, J. Leonhardt, G. Diener, L. De Cola, C. A. Strassert, *Chem. Mater.* **2011**, *23*, 3659.

[24] a) M. J. Burk, J. E. Feaster, W. A. Nugent, R. L. Harlow, *J. Am. Chem. Soc.* **1993**, *115*, 10125; b) I. Bonnaventure, A. B. Charette, *J. Org. Chem.* **2008**, *73*, 6330.

[25] C.-Y. Lin, Y.-C. Lin, W.-Y. Hung, K.-T. Wong, R. C. Kwong, S. C. Xia, Y.-H. Chen, C.-I. Wu, *J. Mater. Chem.* **2009**, *19*, 3618.

[26] K.-C. Hwang, J.-L. Chen, Y. Chi, C.-W. Lin, Y.-M. Cheng, G.-H. Lee, P.-T. Chou, S.-Y. Lin, C.-F. Shu, *Inorg. Chem.* **2008**, *47*, 3307.

[27] P. J. Hay, W. R. Wadt, *J. Chem. Phys.* **1985**, *82*, 299.